

UC Riverside

UC Riverside Previously Published Works

Title

Single-Cell Profiling of Fatty Acid Uptake Using Surface-Immobilized Dendrimers

Permalink

<https://escholarship.org/uc/item/52m7t7df>

Journal

Journal of the American Chemical Society, 143(29)

ISSN

0002-7863

Authors

Guo, Zhili
Cheng, Hanjun
Li, Zhonghan
[et al.](#)

Publication Date

2021-07-28

DOI

10.1021/jacs.1c05103

Peer reviewed



Published in final edited form as:

J Am Chem Soc. 2021 July 28; 143(29): 11191–11198. doi:10.1021/jacs.1c05103.

Single-cell profiling of fatty acid uptake using surface-immobilized dendrimers

Zhili Guo^{#†}, Hanjun Cheng^{#‡}, Zhonghan Li[†], Shiqun Shao^{†,‡}, Priyanka Sarkar[†], Siwen Wang[†], Rohit Chaudhuri[†], Nicole G. Perkins[†], Fei Ji[†], Wei Wei^{‡,*}, Min Xue^{†,*}

[†]Department of Chemistry, University of California, Riverside, Riverside, California 92521, United States

[‡]Institute for Systems Biology, Seattle, Washington 98109, United States

[#] These authors contributed equally to this work.

Abstract

We present a chemical approach to profile fatty acid uptake in single cells. We use azide-modified analogs to probe the fatty acid influx and surface-immobilized dendrimers with dibenzocyclooctyne (DBCO) groups for detection. A competition between the fatty acid probes and BHQ2-azide quencher molecules generates fluorescence signals in a concentration-dependent manner. By integrating this method onto a microfluidics-based multiplex protein analysis platform, we resolved the relationships between fatty acid influx, oncogenic signaling activities, and cell proliferation in single glioblastoma cells. We found that p70S6K and 4EBP1 differentially correlated with fatty acid uptake. We validated that co-targeting p70S6K and fatty acid metabolism synergistically inhibited cell proliferation. Our work provided the first example of studying fatty acid metabolism in the context of protein signaling at single-cell resolution and generated new insights into cancer biology.

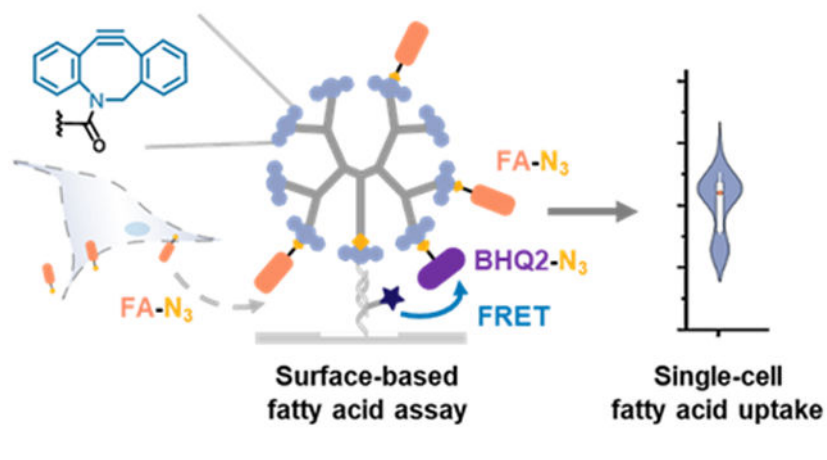
Graphical Abstract

*Corresponding Author wwei@systemsbiology.org (WW); minxue@ucr.edu (MX).

Supporting Information

Development, synthesis and characterization of the dendrimer probes and BHQ2-N₃, operation of SCBC, cell culture, data analysis and other experimental details (PDF). This information is available free of charge on the ACS Publications website.

The authors declare no competing financial interests.



INTRODUCTION

Similar to glucose and amino acids, fatty acids are a major energy source required for sustaining cellular growth and proliferation.¹ Abnormal fatty acid metabolism is frequently observed in cancer, but its regulatory mechanisms and therapeutic implications are unclear. Compared with the well-studied glucose and amino acid metabolic patterns in cancer cells²⁻³, altered fatty acid metabolism received less attention, and current research primarily focuses on the *de novo* fatty acid synthesis pathway⁴. However, increasing evidence has demonstrated that cancer cells' survival and metastatic spreading often require exogenous fatty acid uptake and consumption, even in cells exhibiting high lipogenic activities⁵⁻¹⁰. In addition, fatty acid metabolism in tumor cells exhibits significant plasticity - even the same set of cells can alter their fatty acid dependence in response to drug or environmental stress.^{9, 11} These studies highlight the relevance and complexity of fatty acid metabolism in cancer and necessitate more comprehensive research.

The study of cancer cell metabolism can be confounded by prominent cellular heterogeneity. The causes of this heterogeneity include genetic diversity, signaling and metabolic pathway redundancy, and local microenvironment variations. Such heterogeneity enables metabolic flexibility and promotes tumor progression. On the other hand, these metabolic abnormalities also render tumor cells more vulnerable to metabolic perturbations, which may be exploited therapeutically^{9, 12-13}. Therefore, deciphering cancer cell metabolism, especially in the context of oncogenic signaling heterogeneity, promises the rational design of combinatory therapies for synergistic intervention. Such a task calls for a multiplex single-cell analytical assay that can simultaneously profile metabolic activity and protein levels.

To address this need, we have previously implemented the single-cell barcode chip (SCBC) technology to perform simultaneous analysis of glycolysis, glutamine metabolism, and oncogenic signaling activities at single-cell resolution.¹⁴⁻¹⁶ Nevertheless, a single-cell method to study fatty acid influx on the SCBC platform remains elusive. The technological challenge is the lack of an appropriate fatty acid surrogate that can faithfully report the fatty acid influx while being easy to detect at low concentrations. Fluorescently labeled fatty acid analogs, such as the BODIPY-fatty acids,¹⁷ are widely used and straightforward to detect.

However, they may not faithfully resemble the natural fatty acids in complex biological systems. Isotope-labeled fatty acid surrogates, such as ^{18}F -fluoro-pivalic acid, can perfectly mimic natural fatty acids¹⁸, but their single-cell implementation is challenging. Herein, we choose azide-modified fatty acids (FA- N_3) as surrogates and demonstrate a surface-based chemical method for detecting fatty acid uptake at single-cell resolution. The azide group is chemically inert, and its small size promises a better mimicry to natural fatty acids. We further adapt this method to the SCBC platform to achieve the multiplex analysis of fatty acid uptake with critical signaling proteins from the same single cancer cells.

RESULTS AND DISCUSSION

Design and synthesis of the DBCO dendrimer.

Our fatty acid uptake analysis design is shown in Figure 1. Cells take up the FA- N_3 and then release them upon lysis. The released analogs can then be quantified through a surface-based competition assay. To implement such a design, the azide-bearing analogs must be efficiently captured on the surface. A straightforward method for detecting these azide-bearing analogs is to use the azide-alkyne click chemistry. Because we aimed to multiplex the fatty acid uptake analysis with protein profiling, we cannot use Cu to catalyze the click reaction due to its incompatibility with our immunofluorescence-based SCBC platform. Consequently, we must resort to Cu-free click chemistry, i.e., strain-promoted azide-alkyne cycloaddition (SPAAC). However, azide-based SPAAC chemistry is limited by its low reaction rate. Even with the best reactant – dibenzocyclooctyne (DBCO), the rate constant is only $0.31 \text{ M}^{-1} \text{ S}^{-1}$.¹⁹ Such a reaction rate is not suitable for detecting the low amount of azide-modified fatty acids in single cells. For instance, $50 \mu\text{M}$ azide-fatty acid and $10 \mu\text{M}$ DBCO-COOH lead to negligible reactions after 3 hours of incubation, which is already considered long for a bioassay (Figure S1).

In order to improve the SPAAC reaction rate, we proposed to increase the local DBCO concentration. We hypothesized that a dendritic structure terminated with densely packed DBCO groups could effectively capture the azide-modified fatty acids on the surface (Figure 1b). Nevertheless, closely packed DBCO groups will exhibit prominent hydrophobicity, which also makes it challenging to implement this detection in an aqueous environment.

To overcome the hydrophobicity problem, we proposed to conjugate the dendrimer to a single-strand DNA oligomer (ssDNA). This conjugation also helps to make the SPAAC-based detection compatible with the SCBC platform. We first synthesized G-3 and G-4 dendrimer scaffolds using lysine as building blocks and appended azido-lysine and polyethylene glycol [Lys(N_3)-PEG] linkers (Figure 2a, Figure S2-9). We then conjugated the dendrimers to an ssDNA oligomer through an SPAAC reaction (Figure 2b, Figure S10-12). Lastly, we installed DBCO groups on the dendrimer and obtained the dendrimer-DNA conjugate (Figure 2c, Figure S13, S14). It is worth pointing out that it was critical not to introduce DBCO groups until the very last step, or the strong hydrophobicity of the DBCO groups would prevent the subsequent DNA conjugation (Figure S15-17).

Validation of the proposed competition assay mechanism.

In our proposed detection scheme (Figure 1), the dendrimer-ssDNA conjugate has an embedded Cy3 moiety that provides a fluorescence signal. This signal can be quenched later by a BHQ2-N₃ molecule through the Förster resonance energy transfer (FRET) mechanism. This BHQ2-N₃ molecule can be synthesized through the SPPS process (Figure S18, S19). As the number of FA-N₃ molecules increases, more DBCO sites are occupied and the chance of having a BHQ2-N₃ molecule on the dendrimer decreases. Therefore, FA-N₃ molecules can help retain the Cy3 fluorescence. The more FA-N₃ molecules there are, the higher the fluorescence intensity is. In this manner, the amount of FA-N₃ correlates with the retained fluorescence.

To validate our design, we prepared a mini well surface assay device (Figure 3a). This device has two parts: a polydimethylsiloxane (PDMS) elastomer slab with mini wells and a glass slide with ssDNA patterned on the surface. Because of the complementary sequences, this surface-patterned ssDNA enables the immobilization of the DBCO-ssDNA conjugate. With this fully assembled assay device, we could test our proposed reactions by assessing the Cy3 fluorescence on the surface.

We first tested if the DBCO dendrimer could successfully capture the BHQ2-N₃ molecule. As shown in Figure 3b, the surface fluorescence signals decreased significantly after BHQ2-N₃ incubation, which proved that BHQ2-N₃ successfully reacted with the DBCO moieties on the dendrimer and quenched the Cy3 fluorescence. This result supported our hypothesis that the dendrimer structure could increase the local DBCO concentration and capture azide-bearing molecules efficiently. It is also worth noting that the G-4 dendrimer led to a slightly stronger quenching result, which was expected due to its higher DBCO concentration. Nevertheless, considering that the G-4 dendrimer was more difficult to synthesize than the G-3 one and that the difference in the quenching efficiency was not prominent, we decided to use the G-3 dendrimer for the subsequent studies. To prove that the dendrimer structure was necessary, we also performed a similar experiment using a Cy3-ssDNA presenting only one DBCO group. In this case, the fluorescence was not effectively quenched (Figure S20).

Because FA-N₃ and BHQ2-N₃ are expected to compete for the DBCO sites, the resulted fluorescence readout in response to the FA-N₃ amount should be adjustable by changing the BHQ-N₃ concentrations. To identify an optimal quencher concentration, we evaluated how different concentrations of BHQ-N₃ competed with 100 μM of FA-N₃ (azidopentanoic acid, Figure 3c). We chose 0.5 μM as the best BHQ-N₃ concentration because it led to significant, but not complete, quenching of the Cy3 signal, which would allow the detection of lower FA-N₃ concentrations. Using this quencher concentration, we generated a fluorescence response curve by varying the concentrations of the FA-N₃ (Figure 3d). We confirmed that this method could detect FA-N₃ at the μM-level, which was expected to be suitable for the single-cell profiling of fatty acid uptake.²⁰

In vitro implementation of the fatty acid uptake assay.

We tested our detection scheme using U87VIII cells as our model system. These are human glioblastoma cells that exhibit constitutively amplified oncogenic signaling activities and

harbor prominent metabolic plasticity. We first incubated these cells with varying concentrations of the azidopentanoic acid probe and confirmed that the probe was well-tolerated by the cells (Figure 3e). To identify a suitable FA-N₃ concentration that would generate signals within the assay dynamic range, we used our dendrimer-DNA conjugate / BHQ2-N₃ system to evaluate the surrogate uptake at the bulk level. The results (Figure 3f) showed that the cells took up the FA-N₃ probe in a concentration-dependent manner, and the signal leveled off above 10 mM of FA-N₃. This saturation pattern supported the active transportation of the FA-N₃ probe, which was consistent with the pentanoic acid uptake mechanism. Taken together, these results indicated that incubating the cells with 5 mM FA-N₃ was optimal for this assay.

Because of their hydrophobic tails, fatty acids may insert into the cell membrane. This partition is not an active transportation process and may confound our analysis. On the other hand, we expected that the inserted probe molecules would remain in the membrane fragments upon cell lysis and not be detected by our assay. To assess this potential interference, we incubated the cells with the FA-N₃ probe at 4 °C and used our platform to quantify the FA-N₃ in the cells. At such a low temperature, the cells would stop the active transportation of the probe, and any observed signal would originate from the nonspecific insertion into the cell membrane. As expected, the resulted signal was indistinguishable from the control (Figure 3g). To rule out the possibility that the low-temperature treatment dampened the rate of the nonspecific insertion, we performed another experiment where we fixed the cells and then incubated them with the FA-N₃ probe at 37 °C. Again, the resulted signal was not different from the lysate control (Figure 3g). Collectively, these results proved that our assay was specifically reporting the FA-N₃ probes that were actively taken up by the cells.

Single-cell implementation of the fatty acid uptake assay.

We then moved on to incorporate the fatty acid uptake assay onto the SCBC platform.¹⁴ The SCBC has two parts, a two-layer PDMS microfluidic device and a glass slide with patterned ssDNA barcode stripes. The device has 416 programmable microchambers that can trap and segregate single cells. These chambers allow on-chip cell lysis, and they are coupled with the DNA barcode stripes that enable multiplex fluorescence measurements (Figure 4a, Figure S21, S22). Here, the dendrimer-ssDNA conjugate was introduced to the microfluidics chambers and immobilized onto the surface through DNA hybridization, similar to the mini well assay described above. Using the SCBC device, we first confirmed that the nonspecific interaction between the FA-N₃ probe and the PDMS device was negligible (Figure S23). We then generated a fluorescence response curve by varying the FA-N₃ concentration (Figure 4b). The result demonstrated improved sensitivity compared with the mini well assay, consistent with our prior observations on the SCBC platform. The contributing factors include the high-efficiency flow-based washing that decreased the background and the confined chambers that promoted surface binding. Using the 3SD/slope method, we estimated the limit of detection to be 2 nM.

The dendrimer-ssDNA conjugate can be mixed with a cocktail of antibody-ssDNA conjugates to enable multiplex quantitation. As a proof of concept, we quantified the

azidopentanoic acid uptake, critical signaling protein levels, and cell proliferation marker (Ki67) in U87VIII single cells. As shown in Figure 4c, fatty acid uptake abilities varied significantly among cells. Using the standard curve described above, we were able to calculate the fatty acid concentrations in the chambers, which ranged from high nM to low μ M. Considering that the chamber volume was 2 nL, we calculated that each cell took up low fmol-level FA-N₃ molecules, reaching a high μ M to low mM intracellular concentration (Figure S24). We further investigated if the FA-N₃ uptake was dictated by the cell volume. As shown in Figure 4d, there was no obvious correlation between them (Spearman correlation $r = 0.17$, $p = 0.06$; Pearson correlation $r = 0.03$, $p = 0.72$). This result was expected because we have proven above that our assay only detected the probe molecules that resulted from active transportation, whose rate was not necessarily linked to the cell size.

Analysis of the multiplex single-cell dataset.

In order to better compare the heterogeneity among analytes, we standardized the raw data (Figure 4c) to generate a Z-score violin plot (Figure 4e), which provided a direct visualization of the analyte distribution. We found that the fatty acid uptake heterogeneity was different from those associated with signaling proteins. Most notably, fatty acid uptake had no outliers ($|Z| > 2$), while all the protein levels showed outliers, many of which even extended beyond $Z = 4$. The distribution of fatty acid uptake also exhibited two subpopulations corresponding to low ($Z < -1$) and high ($Z > 0$) uptake activities. Such a clear subpopulation separation was not observed in the protein levels. Moreover, this fatty acid uptake distribution was different from the glucose and glutamine uptake results in our previous studies on the same cell line.¹⁴⁻¹⁵

To further investigate the subpopulations, we performed agglomerative hierarchical clustering analysis (Figure 5a). Based on the clusters' analyte levels (Figure 5a,b), we found that cells with high fatty acid uptake exhibited low oncogenic signaling activities (p-EGFR, p-ERK, p-Src and p-Akt). This divergence pointed to a compensatory relationship between glycolysis and fatty acid metabolism. We also noticed that the levels of the cell proliferation marker, Ki67, did not vary between the two subpopulations. This result indicated that neither oncogenic signaling nor fatty acid metabolism was strongly associated with cell proliferation. Such an observation was consistent with our previous studies.¹⁴⁻¹⁵

In order to better evaluate how each analyte contributed to the global cellular heterogeneity, we performed principal component analysis (Figure 5c). We found that PC1 was primarily populated by oncogenic phosphoproteins, including p-Akt, p-ERK, p-Src, etc, while fatty acid uptake was aligned along PC2 with minimal contribution to PC1. This orthogonality between fatty acid uptake and critical oncogenic signaling matched with our clustering results as well as previous studies on GBM. GBM is known to be a highly glycolytic malignancy driven by its commonly altered protein signaling in EGFR/PI3K/Akt and MAPK/ERK pathways.² Activation of EGFR and downstream PI3K/Akt signaling in many GBM cells directly drives cellular glucose uptake and glycolysis by enhancing both the transcriptional expression and translocation to the cell surface of glucose transporters (GLUTs) as well as activating several enzymes in the glycolytic pathway, including

hexokinase and PKM2.²¹⁻²³ The MAPK/ERK signaling can also promote aerobic glycolysis via induction of transcriptional factor c-Myc.²⁴ GBM cells have been reported to be mostly relying on glycolysis as the primary source of ATP in standard culture conditions.²⁵ Therefore, it was not surprising that fatty acid uptake was relatively decoupled from those oncogenic signaling that primarily drives glucose metabolism under normal culture conditions.²⁵⁻²⁷ Moreover, we observed a strong divergence between fatty acid uptake and p-p70S6K, as well as a correlative relationship between fatty acid uptake and p-4EBP1. Because p70S6K and 4EBP1 are two main effectors downstream of mTOR,²⁸ these findings hinted that fatty acid uptake was regulated by mTOR signaling, possibly differentially controlled by the 4EBP1 and S6K axes. These results were consistent with the critical role of mTOR signaling in lipid homeostasis and fatty acid metabolism as well as the observation that p70S6K and 4E-BP1 are independently regulated and they differentially control cellular growth in cancer.²⁹⁻³² Nevertheless, PC1 and PC2 only collectively captured half of the global cellular heterogeneity variance (Figure S25). Therefore, the conclusions drawn from analyzing PC1 and PC2 required further support.

We then sought to scrutinize the interactions between analytes. We calculated the pairwise Spearman correlation values among all analytes, and the result is shown in Figure 5d. We found strong correlations between the signaling proteins, which were indicative of highly coordinated oncogenic signaling network activities and consistent with our previous studies on U87VIII cells. Notably, fatty acid showed negative correlations with p-p70S6K and p-EGFR. P70S6K is a downstream target of mTOR Complex 1 (mTORC1) – a critical regulator of cell proliferation and protein synthesis. Increasing evidence has revealed that tumor cells can uncouple glycolysis from mitochondrial oxidation, allowing the use of additional fuel sources, such as amino acids and fatty acids, to meet their heightened metabolic needs.^{2, 33-34} GBM cells are also capable of utilizing fatty acid metabolism to generate ATP to maintain their survival under nutrient deprivation or therapeutic stress that limits their glucose consumption.²⁵ The anticorrelations between fatty acid uptake and EGFR/mTORC1 signaling echo the previously observed bioenergetic reprogramming towards fatty acid metabolism upon oncogene inhibition or cytostatic treatment in GBM.³⁵⁻³⁶ Based on the strong anticorrelation between fatty acid uptake and p-p70S6K, we further hypothesized that co-inhibiting p70S6K and fatty acid metabolism would synergistically inhibit cell proliferation.

To test our hypothesis, we treated U87VIII cells with LY2584702 (a p70S6K inhibitor), trimetazidine (a fatty acid metabolism inhibitor), and a combination of them (Figure 6a). It was evident that the combination synergistically inhibited cell proliferation (Figure 6b, Figure S26). To quantitatively evaluate this synergy, we treated the cells with drugs under a concentration titration and calculated the synergy score using the BLISS definition of independence. As shown in Figure 6c, we observed strong synergy between the two drugs across a wide range of concentrations. This result supported our hypothesis that p70S6K negatively regulated fatty acid metabolism in U87VIII cells. We further confirmed that such a synergistic therapy was also applicable to the parent *EGFR* wild-type U87 and patient-derived GBM neurosphere GBM39 cells, suggesting that the observed anticorrelation between fatty acid uptake and mTORC1 may also exist in other GBM cells, independent of *EGFR* mutational status (Figure S27).

CONCLUSION

In conclusion, we established a dendrimer-based detection scheme for profiling fatty acid uptake in single cells. When integrated into the multiplex single-cell barcode chip platform, we were able to perform simultaneous analysis of fatty acid uptake and critical oncogenic signaling proteins in single cells. Using this technology, we identified 4EBP1 and p70S6K as potential regulators of fatty acid metabolism. We found that co-targeting p70S6K and fatty acid metabolism could synergistically inhibit U87VIII proliferation. The technology presented here can be extended to identify other potential regulatory mechanisms of fatty acid metabolism by including additional proteins into the panel, given that the appropriate antibody pairs are available. In addition, the dendrimer-based platform can be easily adapted to detect other azide-modified small molecules.

Supplementary Material

Refer to Web version on PubMed Central for supplementary material.

ACKNOWLEDGMENT

The authors thank the funding support from the National Cancer Institute R03 CA227352 (M.X., W.W.), U54 CA199090 (M.X., W.W.), U01 CA217655 (W.W.), and Andy Hill CARE Fund (W.W.)

REFERENCES

1. Currie E; Schulze A; Zechner R; Walther TC; Farese RV Jr., Cellular fatty acid metabolism and cancer. *Cell Metab* 2013, 18 (2), 153–61. [PubMed: 23791484]
2. Pavlova NN; Thompson CB, The Emerging Hallmarks of Cancer Metabolism. *Cell Metab* 2016, 23 (1), 27–47. [PubMed: 26771115]
3. Martinez-Outschoorn UE; Peiris-Pages M; Pestell RG; Sotgia F; Lisanti MP, Cancer metabolism: a therapeutic perspective. *Nat Rev Clin Oncol* 2017, 14 (1), 11–31. [PubMed: 27141887]
4. Carracedo A; Cantley LC; Pandolfi PP, Cancer metabolism: fatty acid oxidation in the limelight. *Nat Rev Cancer* 2013, 13 (4), 227–32. [PubMed: 23446547]
5. Kamphorst JJ; Cross JR; Fan J; de Stanchina E; Mathew R; White EP; Thompson CB; Rabinowitz JD, Hypoxic and Ras-transformed cells support growth by scavenging unsaturated fatty acids from lysophospholipids. *Proc Natl Acad Sci U S A* 2013, 110 (22), 8882–7. [PubMed: 23671091]
6. Raynor A; Jantschke P; Ross T; Schlesinger M; Wilde M; Haasis S; Dreckmann T; Bendas G; Massing U, Saturated and mono-unsaturated lysophosphatidylcholine metabolism in tumour cells: a potential therapeutic target for preventing metastases. *Lipids Health Dis* 2015, 14, 69. [PubMed: 26162894]
7. Beloribi-Djefafliia S; Vasseur S; Guillaumond F, Lipid metabolic reprogramming in cancer cells. *Oncogenesis* 2016, 5, e189. [PubMed: 26807644]
8. Liu Y; Zuckier LS; Ghesani NV, Dominant uptake of fatty acid over glucose by prostate cells: a potential new diagnostic and therapeutic approach. *Anticancer Res* 2010, 30 (2), 369–74. [PubMed: 20332441]
9. Bensaad K; Favaro E; Lewis CA; Peck B; Lord S; Collins JM; Pinnick KE; Wigfield S; Buffa FM; Li JL; Zhang Q; Wakelam MJ; Karpe F; Schulze A; Harris AL, Fatty acid uptake and lipid storage induced by HIF-1alpha contribute to cell growth and survival after hypoxia-reoxygenation. *Cell Rep* 2014, 9 (1), 349–65. [PubMed: 25263561]
10. Camarda R; Zhou AY; Kohnz RA; Balakrishnan S; Mahieu C; Anderton B; Eyob H; Kajimura S; Tward A; Krings G; Nomura DK; Goga A, Inhibition of fatty acid oxidation as a therapy for MYC-overexpressing triple-negative breast cancer. *Nat Med* 2016, 22 (4), 427–32. [PubMed: 26950360]

11. Du J; Su Y; Qian C; Yuan D; Miao K; Lee D; Ng AHC; Wijker RS; Ribas A; Levine RD; Heath JR; Wei L, Raman-guided subcellular pharmaco-metabolomics for metastatic melanoma cells. *Nat Commun* 2020, 11 (1), 4830–4830. [PubMed: 32973134]
12. Tateishi K; Iafrate AJ; Ho Q; Curry WT; Batchelor TT; Flaherty KT; Onozato ML; Lelic N; Sundaram S; Cahill DP; Chi AS; Wakimoto H, Myc-Driven Glycolysis Is a Therapeutic Target in Glioblastoma. *Clin Cancer Res* 2016, 22 (17), 4452–65. [PubMed: 27076630]
13. Hensley CT; Faubert B; Yuan Q; Lev-Cohain N; Jin E; Kim J; Jiang L; Ko B; Skelton R; Loudat L; Wodzak M; Klimko C; McMillan E; Butt Y; Ni M; Oliver D; Torrealba J; Malloy CR; Kernstine K; Lenkinski RE; DeBerardinis RJ, Metabolic Heterogeneity in Human Lung Tumors. *Cell* 2016, 164 (4), 681–694. [PubMed: 26853473]
14. Xue M; Wei W; Su Y; Kim J; Shin YS; Mai WX; Nathanson DA; Heath JR, Chemical methods for the simultaneous quantitation of metabolites and proteins from single cells. *J Am Chem Soc* 2015, 137 (12), 4066–9. [PubMed: 25789560]
15. Xue M; Wei W; Su Y; Johnson D; Heath JR, Supramolecular Probes for Assessing Glutamine Uptake Enable Semi-Quantitative Metabolic Models in Single Cells. *J Am Chem Soc* 2016, 138 (9), 3085–93. [PubMed: 26916347]
16. Li Z; Cheng H; Shao S; Lu X; Mo L; Tsang J; Zeng P; Guo Z; Wang S; Nathanson DA; Heath JR; Wei W; Xue M, Surface Immobilization of Redox-Labile Fluorescent Probes: Enabling Single-Cell Co-Profiling of Aerobic Glycolysis and Oncogenic Protein Signaling Activities. *Angewandte Chemie International Edition* 2018, 57 (36), 11554–11558. [PubMed: 29992724]
17. Huang H; Starodub O; McIntosh A; Kier AB; Schroeder F, Liver fatty acid-binding protein targets fatty acids to the nucleus. Real time confocal and multiphoton fluorescence imaging in living cells. *J Biol Chem* 2002, 277 (32), 29139–51. [PubMed: 12023965]
18. Witney TH; Pisaneschi F; Alam IS; Trousil S; Kaliszczak M; Twyman F; Brickute D; Nguyen QD; Schug Z; Gottlieb E; Aboagye EO, Preclinical evaluation of 3–18F-fluoro-2,2-dimethylpropionic acid as an imaging agent for tumor detection. *J Nucl Med* 2014, 55 (9), 1506–12. [PubMed: 25012458]
19. Debets MF; van Berkel SS; Schoffelen S; Rutjes FPJT; van Hest JCM; van Delft FL, Aza-dibenzocyclooctynes for fast and efficient enzyme PEGylation via copper-free (3+2) cycloaddition. *Chemical Communications* 2010, 46 (1), 97–99. [PubMed: 20024305]
20. Yao C-H; Fowle-Grider R; Mahieu Nathaniel G.; Liu G-Y; Chen Y Jr.; Wang R; Singh M; Potter Gregory S.; Gross Richard W.; Schaefer J; Johnson Stephen L.; Patti Gary J., Exogenous Fatty Acids Are the Preferred Source of Membrane Lipids in Proliferating Fibroblasts. *Cell Chemical Biology* 2016, 23 (4), 483–493. [PubMed: 27049668]
21. Wieman HL; Wofford JA; Rathmell JC, Cytokine Stimulation Promotes Glucose Uptake via Phosphatidylinositol-3 Kinase/Akt Regulation of Glut1 Activity and Trafficking. *Molecular Biology of the Cell* 2007, 18 (4), 1437–1446. [PubMed: 17301289]
22. Elstrom RL; Bauer DE; Buzzai M; Karnauskas R; Harris MH; Plas DR; Zhuang H; Cinalli RM; Alavi A; Rudin CM; Thompson CB, Akt Stimulates Aerobic Glycolysis in Cancer Cells. *Cancer Research* 2004, 64 (11), 3892. [PubMed: 15172999]
23. Liang J; Cao R; Zhang Y; Xia Y; Zheng Y; Li X; Wang L; Yang W; Lu Z, PKM2 dephosphorylation by Cdc25A promotes the Warburg effect and tumorigenesis. *Nat Commun* 2016, 7 (1), 12431. [PubMed: 27485204]
24. Papa S; Choy PM; Bubici C, The ERK and JNK pathways in the regulation of metabolic reprogramming. *Oncogene* 2019, 38 (13), 2223–2240. [PubMed: 30487597]
25. Kant S; Kesarwani P; Prabhu A; Graham SF; Buelow KL; Nakano I; Chinnaiyan P, Enhanced fatty acid oxidation provides glioblastoma cells metabolic plasticity to accommodate to its dynamic nutrient microenvironment. *Cell Death & Disease* 2020, 11 (4), 253. [PubMed: 32312953]
26. Nagarajan SR; Butler LM; Hoy AJ, The diversity and breadth of cancer cell fatty acid metabolism. *Cancer & Metabolism* 2021, 9 (1), 2. [PubMed: 33413672]
27. Caniglia JL; Jalsutram A; Asuthkar S; Sahagun J; Park S; Ravindra A; Tsung AJ; Guda MR; Velpula KK, Beyond glucose: alternative sources of energy in glioblastoma. *Theranostics* 2021, 11 (5), 2048–2057. [PubMed: 33500708]

28. Liu GY; Sabatini DM, mTOR at the nexus of nutrition, growth, ageing and disease. *Nature Reviews Molecular Cell Biology* 2020, 21 (4), 183–203. [PubMed: 31937935]
29. Tsai S-Y; Rodriguez Ariana A.; Dastidar Somasish G.; Del Greco E; Carr Kaili L.; Sitzmann Joanna M.; Academia Emmeline C.; Viray Christian M.; Martinez Lizbeth L.; Kaplowitz Brian S.; Ashe Travis D.; La Spada Albert R.; Kennedy Brian K., Increased 4E-BP1 Expression Protects against Diet-Induced Obesity and Insulin Resistance in Male Mice. *Cell Reports* 2016, 16 (7), 1903–1914. [PubMed: 27498874]
30. Koundouros N; Poulogiannis G, Reprogramming of fatty acid metabolism in cancer. *British Journal of Cancer* 2020, 122 (1), 4–22. [PubMed: 31819192]
31. Ricoult SJH; Manning BD, The multifaceted role of mTORC1 in the control of lipid metabolism. *EMBO Rep* 2013, 14 (3), 242–251. [PubMed: 23399656]
32. Nawroth R; Stellwagen F; Schulz WA; Stoehr R; Hartmann A; Krause BJ; Gschwend JE; Retz M, S6K1 and 4E-BP1 Are Independent Regulated and Control Cellular Growth in Bladder Cancer. *PLOS ONE* 2011, 6 (11), e27509. [PubMed: 22110663]
33. Li Z; Wang Z; Tang Y; Lu X; Chen J; Dong Y; Wu B; Wang C; Yang L; Guo Z; Xue M; Lu S; Wei W; Shi Q, Liquid biopsy-based single-cell metabolic phenotyping of lung cancer patients for informative diagnostics. *Nat Commun* 2019, 10 (1), 3856. [PubMed: 31451693]
34. Anderson NM; Mucka P; Kern JG; Feng H, The emerging role and targetability of the TCA cycle in cancer metabolism. *Protein & Cell* 2018, 9 (2), 216–237. [PubMed: 28748451]
35. Caragher S; Miska J; Shireman J; Park CH; Muroski M; Lesniak MS; Ahmed AU, Temozolomide Treatment Increases Fatty Acid Uptake in Glioblastoma Stem Cells. *Cancers* 2020, 12 (11).
36. Guo D; Prins RM; Dang J; Kuga D; Iwanami A; Soto H; Lin KY; Huang TT; Akhavan D; Hock MB; Zhu S; Kofman AA; Bensinger SJ; Yong WH; Vinters HV; Horvath S; Watson AD; Kuhn JG; Robins HI; Mehta MP; Wen PY; DeAngelis LM; Prados MD; Mellinghoff IK; Cloughesy TF; Mischel PS, EGFR Signaling Through an Akt-SREBP-1–Dependent, Rapamycin-Resistant Pathway Sensitizes Glioblastomas to Antilipogenic Therapy. *Science Signaling* 2009, 2 (101), ra82. [PubMed: 20009104]

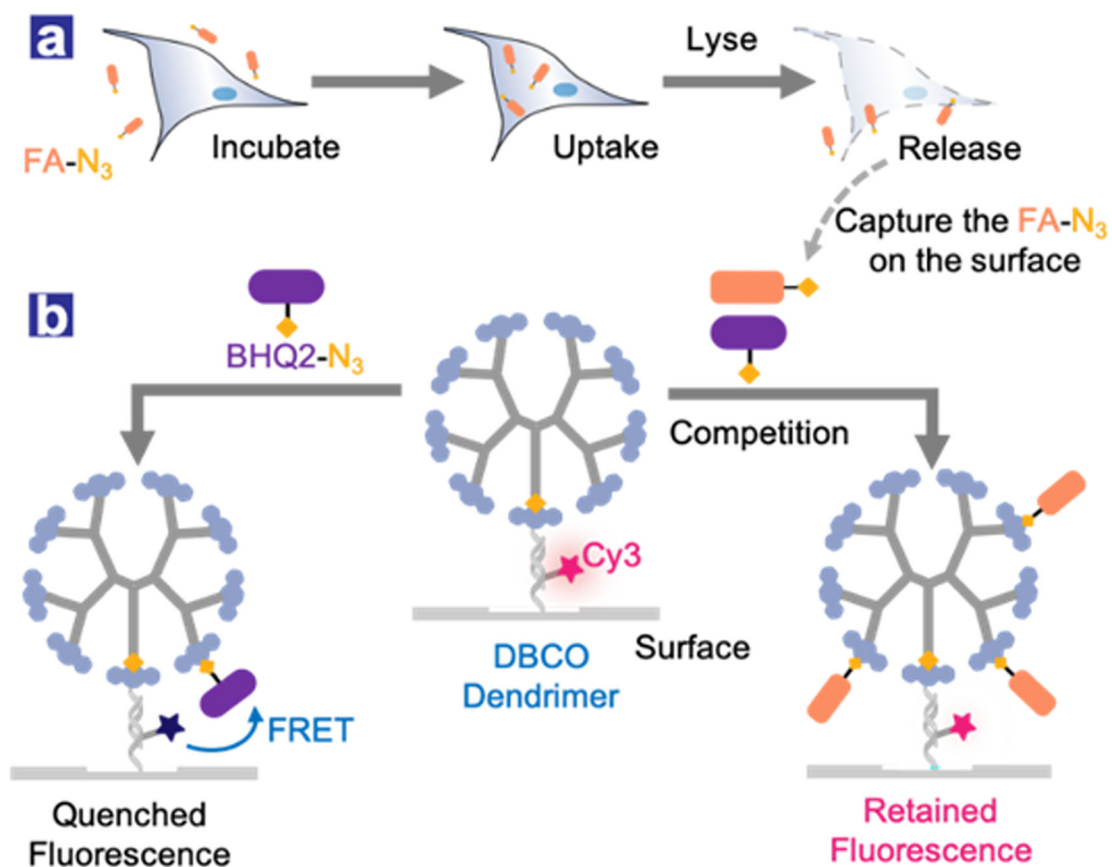


Figure 1. Detecting fatty acid uptake from single cells. (a) Cells take up the azide-modified fatty acid (FA-N₃) molecules and subsequently release them upon lysis. (b) Cy3-modified dibenzocyclooctyne (DBCO) dendrimers capture the released FA-N₃ molecules. The FA-N₃ competes with the BHQ2-N₃ quencher to retain the Cy3 fluorescence.

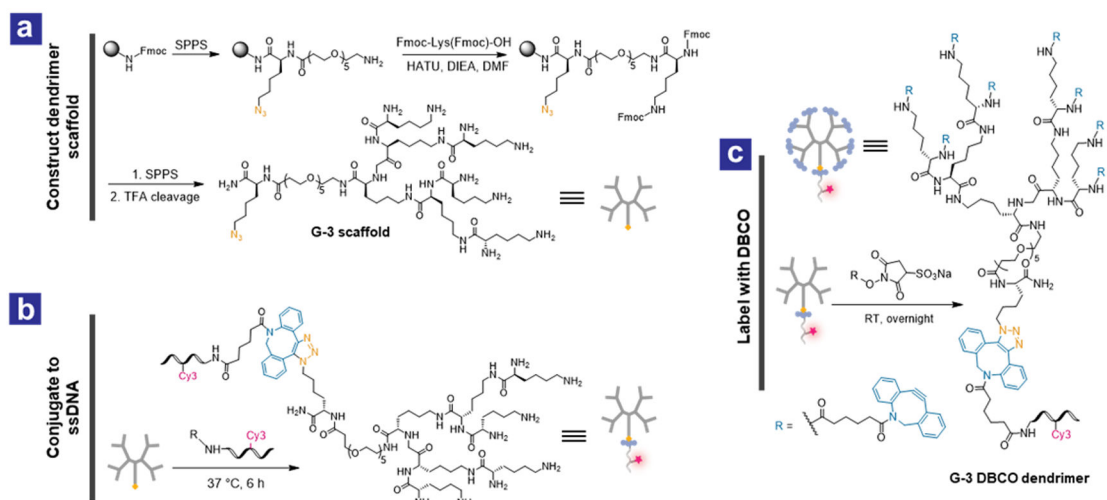
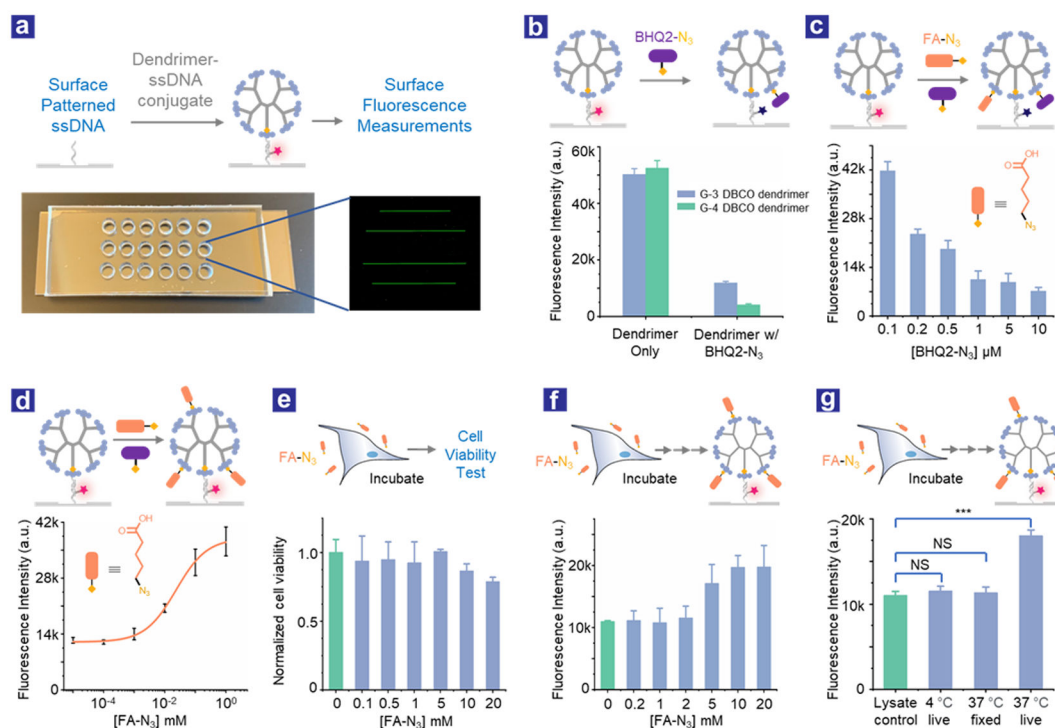


Figure 2.

The synthesis of the G-3 DBCO dendrimer conjugated with Cy3-ssDNA. (a) The amine-bearing G-3 dendritic scaffold was constructed through solid-phase peptide synthesis (SPPS) and then cleaved off from the resin. (b) The scaffold was later conjugated with Cy3-modified ssDNA via SPAAC. (c) Finally, all of the primary amines on the dendrimer scaffold were capped using DBCO-sulfo-NHS ester. G-4 DBCO dendrimer was prepared in a similar manner with an additional round of lysine conjugation.

**Figure 3.**

(a) A picture of the mini well assay device. The size of the glass slide is 75 mm by 26 mm. The PDMS slab provides assay space, and the glass slide enables surface-based detection. The dendrimer-ssDNA conjugate can be immobilized through DNA hybridization. The resulted surface fluorescence can be quantified using a microarray scanner. (b) BHQ2-N₃ effectively reacted with the DBCO dendrimer and quenched the Cy3 fluorescence. Both G-3 and G-4 dendrimers exhibited quenching. (c) Different concentrations of BHQ2-N₃ competing with 100 μM of FA-N₃ for the DBCO dendrimer binding sites. The attachment of BHQ2-N₃ caused quenching of the Cy3 fluorescence. (d) The fluorescence response curve generated by varying the concentrations of the FA-N₃ probe. (e) FA-N₃ (up to 20 mM) was well tolerated by U87VIII cells. (f) Incubating U87VIII cells with varying concentrations of FA-N₃ led to different fluorescence intensities on the dendrimer-based detection platform. (g) Low temperature (4 °C) incubation inhibited the FA-N₃ uptake, and fixed cells did not exhibit uptake either. The cell lysate was used to provide background fluorescence intensity. The error bars in all graphs (b-g) show the standard deviation values calculated from four individual measurements. Student's t-test was used to evaluate the statistical significance. NS: not significant, $p > 0.05$. ***: $p < 0.001$

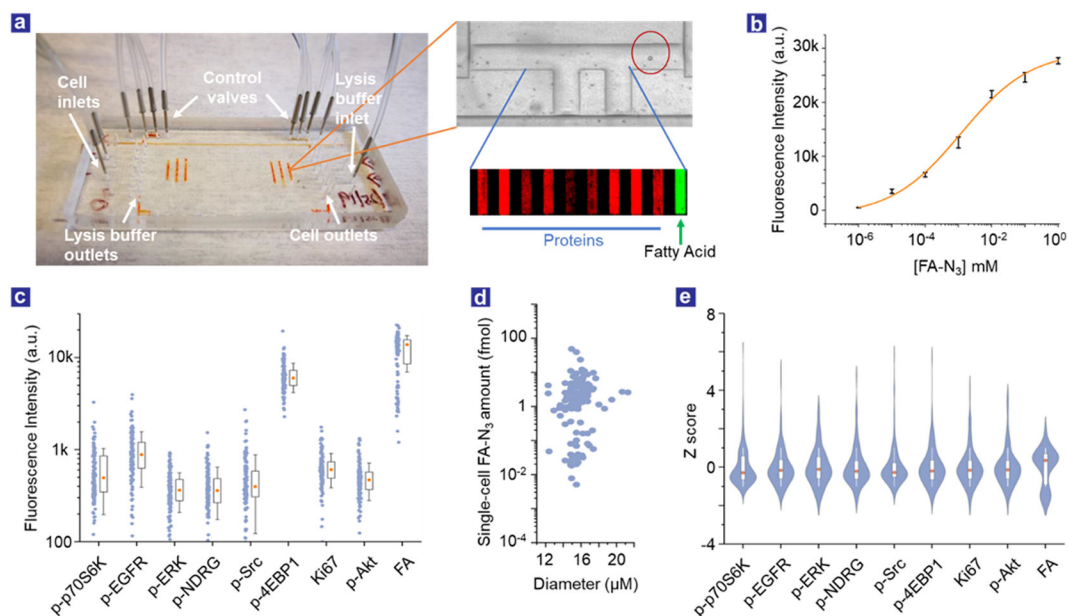


Figure 4.

(a) A picture of the assembled SCBC device. The PDMS microfluidic device contains microchambers that are controlled by the pneumatic valves. The red circle highlights the trapped single U87VIII cell in this example. The glass slides at the bottom contained pre-patterned ssDNA barcode stripes, which enables multiplex immunofluorescence-based protein detection. After the assay, the barcode fluorescence intensities are quantified using a microarray scanner, and the values are extracted and assigned according to the chamber location. A representative fluorescence image of the barcode strips from one single-cell chamber is shown here as an example. (b) The fluorescence response curve generated using different concentrations of the FA- N_3 probe. The error bars show the standard deviation values calculated from four individual measurements. The data points were fitted using a Hill function. (c) The Multiplex single-cell dataset obtained from U87VIII cells. Each dot shows an analyte level obtained from a single cell. The boxes depict the middle two quartiles of the analyte level distributions, and the red dots represent the median values. A total of 151 single cells were assayed using two SCBC devices. (d) The measured fatty acid amount from each single cell against the diameter of the cell. No obvious correlation existed between these two parameters. (e) The violin plots represent the standardized analyte level distributions. The dataset was standardized for each analyte to obtain the Z score of each value. The widths of the violin plots represent the observed frequencies.

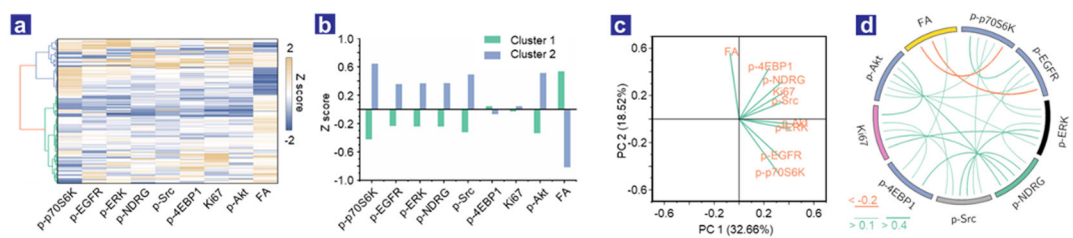


Figure 5.

(a) Agglomerative hierarchical clustering of the single-cell dataset. The standardized single-cell dataset was used as the input. The Euclidean distance values between data points were calculated and tabulated as a matrix. This distance matrix was then used to perform agglomerative hierarchical clustering using Ward's method. Each small bar represents one single-cell data point, and the color represents the Z score of that data point. This AHC analysis identified two distinct clusters, which are denoted by the blue and green branches in the dendrogram on the left. (b) Analyte levels of the two cluster centroids. A distinct bifurcation was observed for most analytes. (c) The loading plot showing the first two principal components (PC1 and PC2) of the single-cell dataset. The vectors are labeled with the corresponding analyte names, and the vector positions show the loading of the analytes in each PC. (d) The correlation network of the analytes. The Spearman correlation values were calculated between each analyte pair. Orange and green lines represent negative and positive correlations, respectively. The line thickness corresponds to the correlation level.

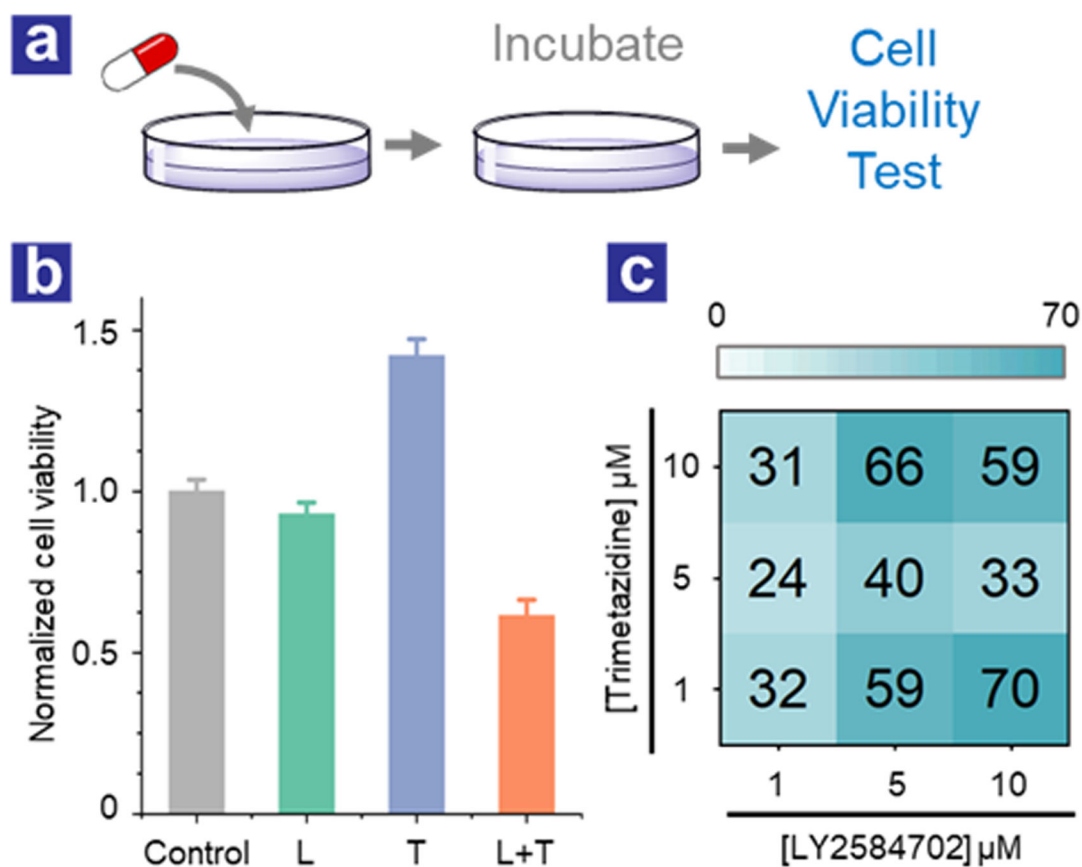


Figure 6. (a) Illustration of the experimental procedure. (b) U87VIII cell viabilities as results of LY2584702 (p70S6K inhibitor, 10 μM) and trimetazidine (fatty acid metabolism inhibitor, 1 μM) treatments. The error bars show the standard deviation values calculated from three individual samples. (c) Synergy scores calculated from the BLISS method across different concentrations of trimetazidine and LY2584702 combinations.